HHS Public Access

Author manuscript

J Autoimmun. Author manuscript; available in PMC 2022 February 01.

Published in final edited form as:

J Autoimmun. 2021 February ; 117: 102581. doi:10.1016/j.jaut.2020.102581.

Subjects at-risk for future development of rheumatoid arthritis demonstrate a PAD4- and TLR-dependent enhanced histone H3 citrullination and proinflammatory cytokine production in CD14^{hi} monocytes

Yuko Okamato[1,2], **Tusharkanti Ghosh**[3], **Tsukasa Okamoto**[4], **Ronald P. Schuyler**[5], **Jennifer Seifert**[1], **Laura Lenis Charry**[1], **Ashley Visser**[1], **Marie Feser**[1], **Chelsie Fleischer**[1], **Chong Pedrick**[1], **Justin August**[1], **Laurakay Moss**[1], **Elizabeth A. Bemis**[6], **Jill M. Norris**[6], **Kristine A. Kuhn**[1], **M. Kristen Demoruelle**[1], **Kevin D. Deane**[1], **Debashis Ghosh**[3], **V. Michael Holers**[1,+], **Elena W.Y. Hsieh**[5,7,+]

[1]University of Colorado Denver, Division of Rheumatology, Aurora, CO, USA

[2]Tokyo Women's Medical University School of Medicine, Department of Rheumatology, Tokyo, Japan

[3]Colorado School of Public Health, Department of Biostatistics and Informatics, Aurora, CO USA

[4]University of Colorado Denver, Department of medicine, Aurora, CO, USA

[5]University of Colorado School of Medicine, Department of Immunology and Microbiology Aurora, CO, USA

[6]Colorado School of Public Health, Department of Epidemiology, Aurora, CO, USA

[7]University of Colorado School of Medicine, Children's Hospital Colorado, Department of Pediatrics, Section of Allergy & Immunology, Aurora, CO, USA

Abstract

The presence of anti-citrullinated protein/peptide antibodies (ACPA) and epitope spreading across the target autoantigens is a unique feature of rheumatoid arthritis (RA). ACPA are present in the peripheral blood for several years prior to the onset of arthritis and clinical classification of RA. ACPA recognize multiple citrullinated proteins, including histone H3 (H3). Intracellular

Corresponding Author: Yuko Okamoto, MD, Tokyo Women's Medical University, Division of Rheumatology, Address: 10-22 Kawada-cho, Shinjuku-ku, Tokyo 162-0054, JAPAN, okamoto.yuko@twmu.ac.jp, Fax: +81-3-5269-1726.

[+]Co-Senior Authors

AUTHOR CONTRIBUTIONS

YO, VMH, and EWYH designed the study. YO, TO and AV conducted the experiments. TG, RPS and DG analyzed the data. JS, LLC, MF, CF, CP, JA, LM, EAB, JMN, KAK, MKD and KDD recruited donors and conducted study visits. YO, VMH, and EWYH wrote the manuscript.

Conflicts of interest statement: The authors disclose the following potential conflicts: VMH (Consulting with Janssen, Celgene, and BMS); KDD (Consulting with Janssen, BMS, Inova Diagnostics, ThermoFisher and Microdrop); All other authors have declared that no conflict of interest exists.

citrullination of H3 in neutrophils and T cells is known to regulate immune cell function by promoting neutrophil extracellular trap formation and citrullinated autoantigen release as well as regulating the Th2/Th17 T cell phenotypic balance. However, the roles of H3 citrullination in other immune cells are not fully elucidated. We aimed to explore H3 citrullination and cytokine/metabolomic signatures in peripheral blood immune cells from subjects prior to and after the onset of RA, at baseline and in response to *ex vivo* toll-like receptor (TLR) stimulation. Here, we analyzed 13 ACPA (+) subjects without arthritis but at-risk for future development of RA, 14 early RA patients, and 13 healthy controls. We found significantly elevated H3 citrullination in $CD14^{hi}$ monocytes, as well as $CD1c^{+}$ dendritic cells and $CD66^{+}$ granulocytes. Unsupervised analysis identified two distinct subsets in $CD14^{hi}$ monocytes characterized by H3 modification and unique cytokine/metabolomic signatures. $CD14^{hi}$ monocytes with elevated TLR-stimulated H3 citrullination were significantly increased in ACPA (+) at-risk subjects. These cells were skewed to produce TNFα, MIP1β, IFNα, and partially IL-12. Additionally, they demonstrate peptidyl arginine deiminase 4 (PAD4) mediated upregulation of the glycolytic enzyme PFKFB3. These $CD14^{hi}$ monocytes with elevated H3 citrullination morphologically formed monocyte extracellular traps (METs). Taken together, dysregulated PAD4-driven cytokine production as well as MET formation in $CD14^{hi}$ monocytes in ACPA (+) at-risk subjects likely plays an important role in the development of RA via promoting and perpetuating inflammation and generation of citrullinated autoantigens.

Keywords

Rheumatoid arthritis; Monocyte extracellular traps; Histone H3 citrullination; Toll-like receptor; Cytokines; Immunometabolism

1. Introduction

The presence of anti-citrullinated protein/peptide antibodies (ACPA) and epitope spreading across multiple citrullinated autoantigens [1] is a unique feature of seropositive rheumatoid arthritis (RA). ACPA are present in the peripheral blood for several years prior to the onset of arthritis and classified RA [2, 3] in a timeframe termed the pre-RA period of RA in individuals who eventually develop disease [4]. Elevation of multiple cytokines/chemokines in peripheral blood is also observed in pre-RA, and expansion in levels occurs as the development of inflammatory arthritis nears [1, 5, 6]. During the preclinical period, there may be no clinical or histological evidence of arthritis or synovitis [7], nor complement activation in the peripheral blood [8]. Because of these findings, elevations of peripheral circulating cytokine/chemokine levels are thought to reflect ongoing local inflammatory processes taking place outside of the joint.

Extra-articular sites that have been shown to exhibit inflammation include mucosal sites, such as lung, gut, and gingiva in humans [9], as well as secondary lymphoid organs in mice [10, 11]. Cross-sectional studies of ‘at-risk’ individuals (ARI) for future RA development (first-degree relatives of RA patients with or without serum ACPA positivity) identified local production of ACPA in induced sputum. The ACPA production was also associated with mucosal inflammation and marked enhancement of spontaneous sputum neutrophil

extracellular trap (NET) formation and citrullinated histone H3 (cit-H3) expression. Additionally, elevation of multiple cytokines/chemokines such as TNFα, MCP1, MIP1α/β, IL-1, and IL-6 was also observed in the sputum [12]. Although the mechanisms underlying mucosal inflammation in ARI are unclear, studies have suggested that immune dysregulation of the myeloid compartment is characterized by an altered responsiveness to the lung environment. This altered responsiveness initiates and perpetuates mucosal inflammation leading to local and systemic ACPA production [9].

NET formation is a process known to engulf and kill microorganisms through release of bactericidal granule proteins and chromatins such as DNA and histones [13]. A number of proteins decorate NETs, and it is proposed that the NET protein composition differs based on both the basal status of neutrophils and the type of neutrophil activation pathway that is engaged [14, 15]. Post-translational modifications (PTM) such as those induced via NET formation and histone citrullination are well described. Citrullination is catalyzed by peptidylarginine deiminases (PADs). PAD2 and PAD4, which are among five known PAD isoforms, are primarily expressed in human immune cells. Several risk factors related to the development of RA are associated with elevation of PAD activity, such as smoking, genetic polymorphisms (PAD2/4, PTPN22, and TNFAIP3), and the presence of periodontal inflammation [16–21]. ACPA also recognize multiple citrullinated peptides in NETs and induce NETosis [22]. Thus, NET formation could lead to the generation of citrullinated autoantigens, including nuclear and cytoplasmic proteins. Recent studies have demonstrated that B cells from RA patients produce ACPA that recognize citrullinated and acetylated histones [23, 24], which are generated during NET formation and apoptosis. In addition to neutrophils, monocytes [25], macrophages [26], eosinophils [27], mast cells [28], and plasmacytoid dendritic cells (pDCs) [29] can also release intracellular proteins and DNA with cit-H3 into extracellular trap-like structures, though their functions are less established.

Another important process in RA pathogenesis is activation of the toll-like receptor (TLR) pathway [30, 31]. For example, studies of RA synovium have revealed higher expression of TLRs, including TLR2, TLR3, TLR5 TLR7, TLR8 and TLR9 in fibroblasts, macrophages and dendritic cells (DCs) [32, 33]. Peripheral blood DCs derived from RA patients produce more TNFα and IL-6 via TLR2 or TLR4 stimulation as compared to healthy controls (HC) [34]. In a related manner, recent comprehensive analyses of synovial tissues from newly diagnosed RA patients using mass cytometry, single-cell RNA sequencing, and bulk RNA sequencing revealed similar characteristics in multiple immune cells in RA synovial tissue [35]. For example, transcriptomic analysis identified upregulation of the TLR8 pathway with TNFα expression in two monocyte subsets from RA synovial tissues, which are IL-1β^+ pro-inflammatory monocytes and interferon (IFN)-activated monocytes [35]. While these studies have demonstrated the role of TLR activation in the synovial environment, its role in the preclinical development of RA is not fully elucidated.

These accumulating findings regarding the role of TLR activation in RA and H3 citrullination demonstrated in multiple immune cells motivated our study to understand the role of H3 citrullination, systemic cytokine/chemokine production, and metabolomic alternations in steady state (without stimulation, ‘baseline’) and following TLR stimulation in peripheral whole blood. Here, we demonstrate the presence of H3 citrullination in

multiple immune cell types, including $CD14^{hi}$ monocytes, $CD1c^{+}$ DC subsets, and granulocytes following *ex vivo* TLR4 and TLR7/8 simulation. Notably, $CD14^{hi}$ monocytes with elevated H3 citrullination were significantly increased in blood from ARI. Molecular characteristic of these monocytes is similar regardless of disease status, which is skewed to produce TNFα, MIP1β, IFNα and partially IL-12, with upregulation of glycolytic enzyme 6-phosphofructo-2-kinase/fructose-2,6-bisphosphatase 3 (PFKFB3), in a process mediated by PAD4. Additionally, $CD14^{hi}$ monocytes with elevated H3 citrullination morphologically form monocyte extracellular traps (METs). Thus, our findings demonstrate $CD14^{hi}$ monocytes from ACPA (+) ARI have altered responsiveness to TLR stimulation, and suggest that these processes play an important role in the future development of RA via promotion of inflammation and the generation of citrullinated autoantigens.

2. Materials and methods

2.1. Study subjects

Subjects were recruited from the Studies of the Etiologies of RA (SERA) population, which was designed to use clinical and epidemiologic information as well as informative biomarkers to study RA-related autoimmunity during different phases of RA development, with the goal to identify causal mechanisms and develop disease prevention strategies [36, 37]. For the current study, subjects were recruited at the University of Colorado between September 2016 and February 2019. Mass cytometry data were generated from the originally recruited 40 subjects described in Table 1. An additional six healthy subjects and eight ACPA (+) ARI, who were recruited to perform immunofluorescence staining, live cell imaging, and confirmatory analysis by flow cytometry, are described in Table S1.

2.1.1. ARI for RA: We included 13 serum ACPA (+) (CCP3.1 IgG/IgA Inova) subjects without current or prior inflammatory arthritis who were determined to be ‘At-Risk’ for developing RA in the future. Subjects were identified through community health fairs, clinics, or research-based blood test screening.

2.1.2. Early RA: We included 14 serum ACPA (+) (CCP3.1 IgG/IgA Inova) early RA patients (<one year since diagnosis) with clinically active arthritis who met 2010 RA classification criteria based on medical chart review [38].

2.1.3. HC: 13 healthy subjects were recruited through local advertisement. None of these subjects had a history of RA or inflammatory arthritis by examination, were not a first-degree relative of an RA proband, and were serum ACPA (CCP3.1) and RF-IgM negative.

2.2. Study visit and blood collection

All subjects had blood collected at the time of their study visit. ARI and HC had a 68-count joint examination to confirm the absence of inflammatory arthritis. All RA patients had clinically apparent synovitis at study visit. Self-administered questionnaires were used to obtain demographics and smoking history.

2.3. ACPA and RF testing

Sera were tested for ACPA using the CCP3.1 (IgG/lgA) ELISA assay (Inova Diagnostics, San Diego, CA, USA) and CCP3 (IgG) ELISA assay (Inova Diagnostics). The cut-off level for CCP3.1 and CCP3 positivity was based on the manufacturer's recommendations. We also measured the level of serum RF-IgM, RF-lgA, and RF-IgG using ELISA assay (Inova Diagnostics). The cut-off level was determined as <5% of 491 healthy subjects.

2.4. Shared epitope and PTPN22 testing

DNA was extracted from buffy coat of samples from each subject and evaluated for the presence of alleles containing the shared epitope (SE) using previously described methods [36]. The alleles DRB1*04:01, 04:04, 04:05, 04:08, 04:09, and 04:10, and DR1*01:01 and 01:02 were considered as SE containing. The PTPN22 risk allele status was determined by carrying the C1858T single nucleotide polymorphism (SNP) [39, 40].

2.5. Whole blood processing for mass cytometry analysis

At each study visit, freshly drawn heparinized whole blood underwent red blood cell lysis and cells were fixed (BD biosciences, 558049), either just after blood draw (T0) or after *ex vivo* stimulation with TLR ligands, including 0.1 μg/ml LPS-EK (TLR4 ligand, InvivoGen, tlrl-peklps), or 5 μg/ml R848 (TLR7/8 ligand, InvivoGen, tlrl-r848), using previously reported methods [41–43]. Six hour stimulated samples were designated as T6 PBS, T6 LPS, and T6 R848, respectively. Cells were stored at −80°C until mass cytometry analysis.

2.6. Mass cytometry analysis

The antibodies used for mass cytometry analysis are listed in Table S2. Metal conjugated antibodies were purchased from the vendor, or conjugation was performed in house using metal-conjugation kit (Multimetal Labeling Kits, Fluidigm). All antibodies were titrated and validated for mass cytometry analysis. To control for run-to-run variation, two anchor samples were included in every mass cytometry analysis. For each analysis, 18 samples including two anchor samples (T0 and T6 mixture) and 16 samples from four subjects, four conditions each, were barcoded, combined, and surface stained as previously reported [41,42]. Cells were permeabilized by Foxp3/transcription staining buffer (ebioscience, 00-5523-00), intracellularly stained, treated with DNA intercalator, and stored at 4°C until mass cytometry analysis on the following day. Data were acquired on a Helios CyTOF instrument (Fluidigm). Ten batches of mass cytometry analysis were performed over four months. Data were normalized using internal metal isotope bead standards by a previously described method [44]. Files were de-barcoded by the Matlab Debarcoder tool [44]. Acquired data were analyzed by computational analysis and manual gating.

2.7. Batch adjustment

To reduce variability across ten batches and to enable direct comparison of samples run across multiple barcodes, we performed batch adjustment as previously described [45]. For the technical replicate, two anchor samples, one stimulated and one unstimulated, were run in each barcode and used for this procedure.

2.8. PhenoGraph analysis [46]

Each FCS file was manually gated on $CD45^+$ cells, $CD45^+CD66^-$ cells, $CD14^{hi}$ monocytes, and $CD1c^+$ DC subsets. The gating strategy is shown in Figure S2. T-distributed stochastic neighbor embedding (t-SNE) is a dimensionality reduction algorithm. T-SNE visualizes high-dimensional data by giving each datapoint a location in a two dimensional map and enable visualization and comparison of massy cytometry data [47]. For the analysis of $CD45^+$ cells or $CD45^+CD66^-$ cells, t-SNE plots were created using 16 surface markers including CD1c, CD3, CD4, CD8, CD11c, CD14, CD15, CD16, CD19, CD27, CD45RA, CD56, CD66, CD123, CXCR5, and HLA-DR. For the analysis of $CD45^+$ cells, we analyzed T0 conditions from three study groups by PhenoGraph. Subsampled 5000 events per file were analyzed to create t-SNE plots. For the analysis of $CD45^+CD66^-$ cells, we analyzed the files of T6 LPS and T6 R848 conditions jointly. Subsampled 5000 events per file were analyzed, and t-SNE plots were created. Twenty-two functional markers including 20 intracellular molecules, CD69, and CD86 were visualized on each t-SNE plot (Figure 1AB).

For the analysis of gated $CD14^{hi}$ monocytes or $CD1c^+$ DC subsets, cells were clustered on 22 functional markers. Subsampling of 1000 events per sample were performed and three conditions (T6 PBS, T6 LPS, and T6 R848) from three groups were analyzed together to create t-SNE plots (Figure 1C/S4).

2.9. CITRUS analysis [48]

$CD45^+$ cells, $CD14^{hi}$ monocytes, and $CD1c^+$ DCs were analyzed using the CITRUS algorithm, which is a regularized regression analysis of molecular features derived from mass cytometry [42]. CITRUS identifies phenotypically similar cell subpopulations as clusters in high-dimensional datasets in an unsupervised way. CITRUS achieves this automated cluster identification by combining events across all samples and hierarchically clustering events based on phenotypic marker similarity. The association model used for this analysis to detect statistically significant immune signatures from clusters was Nearest Shrunken Centroid based predictive model which was originally developed in PAMR (Prediction Analysis for Microarrays) [49]. The PAMR based CITRUS to test the statistical changes were analyzed in abundance mode. We performed the CITRUS analysis by controlling the False Discovery Rate (FDR = 0.05).

Each file was pre-gated on $CD45^+$ cells, $CD14^{hi}$ monocytes, and $CD1c^+$ DC subsets, respectively. For the analysis of $CD45^+$ cells, gated $CD45^+$ cells were clustered on 16 surface markers including CD1c, CD3, CD4, CD8, CD11c, CD14, CD15, CD16, CD19, CD27, CD45RA, CD56, CD66, CD123, CXCR5, and HLA-DR. Subsampled 1000 events from each file of T0 condition from three study groups were analyzed by CITRUS algorithm. Twenty-two functional markers were visualized on each CITRUS tree. Nodes are scaled on abundance of cells in the cluster and compared between the three study groups. For the analysis of $CD14^{hi}$ monocytes and $CD1c^+$ DCs, T6 LPS and T6 R848 conditions were analyzed separately. Subsampled 10000 events from each file were clustered on 22 functional markers described above. Expression of each functional marker was visualized on each CITRUS tree and abundance of each cluster was compared between three study groups (Figure 2/S5/S6).

2.10. Gating of cit-H3^{hi} population by mass cytometry analysis

Mass cytometry data were manually analyzed using Flowjo software (BD biosciences) and CellEngine software (PRIMITY BIO, INC). The gating strategy for each population is shown in Figure S2. According to identification criteria of monocyte [50], three subsets were gated; CD14^{hi}CD16^{-} monocyte (classical monocyte), CD14^{hi}CD16^{+} monocyte (intermediated monocyte), CD14^{+}CD16^{hi} monocyte (non-classical monocyte). The cut off level for cit-H3 positivity was determined as the 0.5% positivity for each population in T0 samples from 13 HC.

2.11. Cell subpopulation enrichment experiment

CD14^{hi} monocytes and neutrophils were directly sorted from freshly drawn whole blood by negative selection according to manufacturer's protocol (EasySep Direct Human Monocyte Isolation Kit, Stemcell, 19669, and EasySep Direct Human Neutrophil Isolation Kit, Stemcell, 19666), and purity was from 95-98%. PBMC were isolated from freshly drawn blood, and CD1c+ DC were enriched by negative selection using magnetic beads (EasySep Human Myeloid DC Enrichment Kit, Stemcell, 19061); purity was ~90%.

Whole blood was incubated with PBS, 0.1 μg/ml LPS, or 5 μg/ml R848 and processed as described in mass cytometry analysis. PBMC, sorted CD14^{hi} monocytes, granulocytes, and CD1c^{+} DC were incubated with each ligand at a concentration of 1×10^{6} cells/ml in RPMI1640 supplemented with 10% fetal bovine serum (FBS) for six hours at RT and fixed with 1.5% PFA. Cells were surface stained with anti-CD45, CD66, CD3, CD19, HLA-DR, CD14, CD16, and CD1c antibodies, fixed, and permeabilized by Fox3/transcription staining buffer (ebioscience, 00-5523-00) for 30 minutes at RT, and then intracellularly stained with anti-cit-H3 antibody (1:200) or anti-rabbit polyclonal isotype antibody (1:200, abcam, ab171870) which were directly conjugated with R-Phycoerythrin (R-PE) using antibody labeling kit (Expedon, 703-0010) and titrated. Flow cytometry data were acquired on Cytec Aurora (CYTEC). Data were manually analyzed using CellEngine software. The cut off level for the cit-H3^{hi} population was established by 0.1% positivity of the isotype control in each population through flow cytometry analysis.

2.12. Monocyte western blotting

Purified CD14^{hi} monocytes were incubated with PBS or 5 μg/ml R848 for six hours and analyzed by Western blotting for the level of cit-H3, total H3, PAD4, PAD2, and β-actin. Blots were run with samples loaded per total protein level (10 μg of protein per well). A positive control protein was run with each blot that included H3 (Cayman, 10263), PAD4 (Cayman, 10500), and PAD2 (Cayman, 10785). Antibodies were used to detect total H3 (Abcam, ab1791), cit-H3 (citrulline R2+R8+R17, Abcam, ab5103), PAD4 (Abcam, ab128086), PAD2 (Abcam, ab16478), and β-actin (Cell Signaling, 3700). Secondary antibodies included IRDye 680RD Donkey anti-mouse IgG (LI-COR, #925-68072) and IRDye 800CW Donkey anti-Rabbit IgG (LI-COR, #925-32213). Blots were imaged using the LI-COR Odyssey CLx. The quantitative intensity of western blot bands was calculated using Image Studio Lite ver 5.2 (LI-COR). Each band was normalized to the total H3 or β-actin.

2.13. Ex vivo METosis assay by immunofluorescence and IncuCyte ZOOM

Sorted CD14^{hi} monocytes were stimulated and MET formation was characterized and quantified by immunofluorescence [14, 51] and IncuCyte Zoom [52].

2.13.1. Immunofluorescence: Sorted CD14^{hi} monocytes (1×10^6 cells/ml) in RPMI1640 supplemented with 2% FBS were adhered to Poly-D-Lysine coated coverslips in duplicate at 37°C and incubated with PBS or 5 μg/ml R848. Cells were fixed with 4% PFA at 4°C overnight, permeabilized with 0.2% Triton X-100 for 10 minutes, blocked with 10% goat serum, 1% BSA, and Fc block (BD biosciences, 564220). Coverslips were stained with anti-MPO (1:100, 2C7, Abcam, ab25989) and anti-cit-H3 antibodies (1:200, citrulline R2+R8+R17, Abcam, ab5103) or isotype controls at 37°C for one hour followed by incubation with Alexa Fluor 555 conjugated goat anti-mouse IgG antibody (1:100, Invitrogen, A-21424) and Alexa Fluor 647 conjugated goat anti-rabbit IgG antibody (1:100, Invitrogen, A-32733) at 4°C for one hour. Cells were counterstained with ProLong Diamond Antifade Mountant with 4,6-diamidino-2-phenylindole (DAPI, Thermo Fisher, P36966). Confocal microscopy was performed using a Zeiss LSM 780 microscope and images were analyzed with Zen 2 and Adobe Photoshop software.

2.13.2. MET quantification by IncuCyte ZOOM: Metosis was quantified by IncuCyte ZOOM using established protocol for neutrophils [52]. Briefly, sorted CD14^{hi} monocytes were stained with membrane permeable NUCLEAR-ID Red dye (Enzo Life Sciences, ENZ-52406), incubated in 96 well plates in triplicate, and stimulated with 0.1 μg/ml LPS or 5 μg/ml R848. Monocytes undergoing MET formation, which are membrane compromised and consequently Sytox green dye (Thermo Fisher, S7020) positive, were automatically counted.

2.14. Ex vivo stimulation and inhibition assay by flow cytometry

PBMC were stimulated with PBS, 0.1 μg/ml LPS, 5 μg/ml R848, 100 nM Phorbol 12-myristate 13-acetate (PMA), or 1 μg/ml Ionomycin for six hours in the presence of protein transport inhibitor and fixed. H3 citrullination and TNFα production in CD14^{hi} monocytes was analyzed by flow cytometry.

PBMC were pretreated with inhibitors or vesicle for 30 minutes and then stimulated by R848. Inhibitors included BB-Cl-Amidine (pan-PAD inhibitor, Cayman, 17079), GSK484 (PAD4 specific inhibitor, Cayman, 17488), AMF30a (PAD2 specific inhibitor, Cayman, 22653), 3-BP (3-bromopyruvate, hexokinase-2 inhibitor, Millipore sigma, CAS 1113-59-3), and DPI (diphenylene iodonium, NADPH oxidase inhibitor, Tocris, 0504). Stimulated cells were washed twice in PBS, stained with Zombie aqua fixable viable kit (1:1000, Biolegend, 413202) in PBS for 10 minutes, washed twice in PBS, and fixed by 1.5% PFA for 10 minutes at RT. Cells were stained and analyzed by flow cytometry as described above. Anti-CD45, CD3, CD19, HLA-DR, CD14, and CD16 antibodies were used for surface staining, and PE conjugated anti-citH3 antibody or anti-rabbit polyclonal isotype antibody, anti-TNFα, IL-1β, and PERP1 (cleaved Asp214) antibody were included for intracellular staining. Antibodies used for analysis were listed in Table S1. Cut off levels were

determined by 0.1% positivity of cit-H3 isotype control and 5% TNFα or IL-1β positivity of unstimulated CD14^{hi} monocytes.

2.15. Statistical analyses

Subject demographics, cluster abundance created by CITRUS analysis, and frequencies of cell population were compared between groups using Mann-Whitney test for two groups or Kruskal-Wallis test adjusted by Benjamini and Yekutieli method to account for multiple testing, as appropriate. Frequencies of cit-H3^{hi} monocytes were correlated with age, RF-IgM tier, anti-CCP3 titer, and anti-CCP3.1 titer using Spearman's correlation coefficient. Sytox green positive cells by IncuCyte ZOOM and frequencies of cell population in inhibition assay were compared by the Friedman test adjusted by Benjamini and Yekutieli method to account for multiple testing.

2.16. Ethical considerations.

All study procedures were approved by the Colorado Multiple Institutional Review Board, and written informed consent was obtained from all subjects at the study visit.

3. Results

3.1. Study participants demographic and autoantibody profiles

We studied 13 ARI, 14 early RA patients, and 13 HC by mass cytometry analysis. Subject demographics are included in Table 1. Of the 13 ARI, three were a first-degree relative of a RA patient, and 10 were not. Eleven of the ARI were also anti-CCP3 (IgG) antibody positive, four were RF-IgM positive, and two were both RF-IgM and RF-IgA positive, the latter of which suggests an even higher risk of developing RA in the future [5, 53]. Eight of the early RA patients were newly diagnosed before starting disease modifying anti-rheumatic drugs, and six patients were currently taking disease modifying anti-rheumatic drugs.

ARI exhibited a non-significant trend to being older than early RA patients and HC. There was a non-significant trend toward a higher prevalence of a smoking history and SE positivity in early RA patients. There were no significant differences in sex, race, or PTPN22 SNP positivity between groups.

3.2. Immunophenotypic characterization demonstrates a comparable immunological landscape at baseline across ARI, RA, and HC groups

To investigate alterations of immune cell subsets and their functional state, we analyzed freshly drawn peripheral whole blood via mass cytometry, including evaluation of 22 surface markers and 20 intracellular proteins (Methods, Figure S1). Surface markers delineated lymphoid and myeloid cell subsets including T, B, NK, DCs, monocytes, and granulocytes. Intracellular proteins included cytokines, metabolic proteins, and histone modifications. We used PhenoGraph to cluster cells in an unsupervised manner, using surface markers to distinguish immune cell populations and to evaluate expression of intracellular molecules for each population. Additionally, we used CITRUS to identify statistically significant cell population frequency differences across study groups.

At baseline (unstimulated) and following TLR stimulation, the overall immune phenotypic composition was comparable across study groups, as evaluated by PhenoGraph and CITRUS analysis. Concordant with the two unsupervised computational methods, hierarchical gating of specific lymphoid and myeloid immune cell subsets did not identify any statistically significant differences in population frequency (data not shown).

3.3. TLR stimulation upregulates cytokines/chemokines and metabolomic proteins along with H3 modifications in CD14^{hi} monocytes and CD1c^{+} DCs

Given previous studies supporting the role of abnormal immune cellular activation and downstream functional consequences in the development of RA, we further investigated the functional perturbations in specific immune cell subsets across the ARI, early RA, and HC groups. Particularly, upregulation of TLR and downstream cytokine production had been previously described in synovial fluid monocytes, but not yet explored in peripheral circulating immune cell populations in the ARI. Additionally, while PAD-mediated H3 citrullination and its downstream cytokine signatures have been previously studied in neutrophils and T cells, PAD functions and citrullination in other immune cells has not been elucidated. To evaluate differences in cellular functional states between ARI, early RA and HC's peripheral immune cell subsets, we stimulated their peripheral blood samples with TLR4 and TLR7/8 agonists, to mimic extracellular and endoplasmic ligand engagement. Downstream events following engagement of such pathways were assessed, including classic pro-inflammatory cytokines, interferon dependent cytokines, and metabolomic proteins.

Using PhenoGraph to cluster cells into phenotypic subsets (Figure 1A), we evaluated within each cluster (i.e. immune cell subset) expression of cytokines, metabolomic proteins, and PTM states. Upregulation of multiple cytokines/chemokines, and metabolic proteins, such as PFKFB3 in response to LPS and R848 was found in each of the three study groups. Particularly, in CD14^{hi} monocytes and CD1c^{+} DCs, H3 citrullination, H3 phosphorylation, and upregulation of those cytokines/chemokines was identified (Figure 1B). To further focus on this finding, manually gated monocyte populations confirmed that H3 citrullination was induced mainly in CD14^{hi} monocytes, not in intermediate or CD16^{hi} monocytes. H3 citrullination following TLR stimulation was identified in small subsets (<1%) of CD8 T cells, CD4 T cells, B cells, and NK cells but this was not accompanied by upregulation of cytokine or chemokines and their role is unknown.

3.4. H3 citrullination and H3 phosphorylation following TLR stimulation functionally distinguishes two CD14^{hi} monocyte subsets

Since TLR pathway activation has been involved in the synovial inflammation of RA patients, we sought to understand whether this finding was also pervasive in the periphery. Given that CD14^{hi} monocytes demonstrated the greatest upregulation of citrullinated and phosphorylated H3 with downstream cytokine/chemokines production in response to TLR stimulation, we specifically chose to further subset this population based on functional markers.

CD14^{hi} monocytes were clustered on 22 functional markers to dissect this cell population based on different functional states (Figure 1C). These functionally distinctive CD14^{hi} monocyte clusters demonstrated significant differences in their distribution in response to different TLR stimuli, demonstrating that this phenotypically uniform cell population of CD14^{hi} monocytes exhibits a significantly heterogeneous functional response.

Since citrullination is a key feature of RA development, we evaluated H3 citrullination using a validated polyclonal antibody which recognize H3 citrullination at arginine 2+8+17 residues [54]. At baseline in T6 PBS sample, we did not find any clusters with elevated H3 citrullination. Following *ex vivo* TLR stimulation, though, we found in T6 LPS and T6 R848 samples subsets of cells with H3 citrullination accompanied with TNFα, MIP1β, and IL-12 production but no other cytokines and chemokines measured (Figure 1C/S4). This cluster also demonstrated PFKFB3 upregulation, suggesting induction of glycolytic process in these cells. Other stimulated CD14^{hi} monocytes without H3 citrullination displayed H3 phosphorylation at serine 28 residue, instead. H3 phosphorylated CD14^{hi} monocytes produced multiple cytokines/chemokines with PFKFB3 expression. IL-1α/β/RA, 6, 8, 12, TNFα, MIP1β, and MCP1 were commonly produced by H3 phosphorylated cells following stimulation, but IL-23 was upregulated only by LPS, reflecting engagement of unique cytokine pathways following each TLR ligand.

3.5. CD14^{hi} monocyte subsets with different levels of citrullinated H3 modifications demonstrate a unique cytokine profile and are functionally distinct

To further characterize subpopulations of CD14^{hi} monocytes, we segregated this population based on their levels of PTM H3. We used CITRUS to dissect CD14^{hi} monocyte subtypes based on their metabolomic and PTM states, since this algorithm has been previously used to identify specific parameters that best segregate disease versus healthy control subjects based on statistically significant differences on immune marker expression levels [42]. CITRUS analysis of gated CD14^{hi} monocytes in the T6 LPS and T6 R848 condition were performed separately. Following R848 stimulation, two distinct clusters characterized by H3 modification - high H3 citrullination and low H3 citrullination were identified. The latter cluster exhibited H3 phosphorylation and further subdivided into two clusters based on IL-12 expression level (Figure 2A). A summary of each cluster is shown in Table 2. Expression of all functional markers in CITRUS tree is displayed in Figure S6A. Cit-H3^{hi}CD14^{hi} monocytes were significantly increased in ARI and RA compared to HC (Figure 2C), which is characterized by high H3 citrullination and low H3 phosphorylation with TNFα, MIP1β, IFNα, and partially IL-12 production, and glycolytic enzyme PFKFB3 upregulation (Figure 2B). Upregulation of pro-inflammatory cytokines TNFα and IL-12, as well as interferon dependent cytokines (IFNα and MIP1β), suggest a strong pro-inflammatory phenotype. Upregulation of glycolytic enzyme supports the presence of a metabolically active cell status. Cit-H3^{low} population showed high H3 phosphorylation accompanied by IL-1α/β/RA, IL-6, IL-8, TNFα, MCP1, and MIP1β production and PFKFB3 and AMPKα1 upregulation, which is distinctively different from cit-H3^{hi} population.

Additionally, CITRUS analysis of gated CD14^{hi} monocytes in the T6 LPS condition also identified cit-H3 high and low populations with similar molecular characteristics. Cit-H3^{hi}CD14^{hi} monocytes, which is a pro-inflammatory phenotype, were also significantly increased in ARI compared to RA and HC (Figure S5/S6B).

Consistent with two computed analysis, manually gated CD14^{hi} monocytes also demonstrated that H3 citrullination following both LPS and R848 stimulation was significantly enhanced in the ARI compared to the HC (Figure 3AB). RA patients showed significant H3 citrullination following R848 stimulation compared to HC; however there were no differences following LPS simulation. There was no difference in frequencies of CD14^{hi} monocytes in CD66^{-} CD45^{+} singlets among three groups at baseline and T6 PBS conditions (Figure S3A), suggesting that this functional difference is not likely related to phenotypic status but rather a consequence of PTM and metabolomic alterations.

Enhanced cit-H3^{hi}CD14^{hi} monocytes was not significantly associated with gender, race, SE allelles, PTPN22 SNPs, anti-CCP level, and RF-IgM level. Within ARI, frequency of cit-H3^{hi}CD14^{hi} monocytes following R848 stimulation significantly correlated with age (Spearman r=0.73, p=0.007) and this was not observed in LPS condition or other groups (Table S3). There was a non-significant trend towards a higher frequency of cit-H3^{hi}CD14^{hi} monocytes following R848 and LPS stimulation in ever-smokers in all groups, suggesting smoking could enhance this citrullination process regardless of disease status (data not shown).

Other than monocytes, we found a small frequency of a cit-H3^{hi} subpopulation in stimulated CD1c^{+} DCs (~3%) with similar molecular characteristics as cit-H3^{hi}CD14^{hi} monocytes (data not shown). There was a non-significant trend toward a higher frequency of cit-H3^{hi}CD1c^{+} DCs following R848 stimulation in ARI and RA compared to HC, suggesting there might be a similar enhancement of this pathway in ARI and RA (Figure S3B). Although a previous study reported association between TLR simulation and H3 citrullination in neutrophils, we found a slight increase of cit-H3^{hi} popuation in CD66^{+} granulocytes (~0.5%) following stimulation which was not significantly different among the three groups (Figure S3C).

3.6. Cell-intrinsic engagement of TLR pathway induces H3 citrullination in CD14^{hi} monocytes, CD1c^{+} DCs, and neutrophils

To determine if H3 citrullination was induced by endogenous engagement of the TLR pathway within specific cell subsets, we examined H3 citrullination in isolated CD14^{hi} monocytes, CD1c^{+} DCs, and neutrophils, compared to PBMC (affected by celluar interactions) and whole blood (affected by serum circulating factors). Freshly drawn blood from an additional three HC (Table S1) were incubated with PBS, LPS, and R848 for six hours and frequencies of cit-H3^{hi} population in each condition were analyzed by flow cytometry. Gating of cit-H3^{hi} population is shown in Figure 5A/S9A. Representative data from single individual is displayed in Figure S7. H3 citrullination was observed in all stimulated conditions, sorted population, PBMC, and whole blood condition of gated in CD14^{hi} monocytes, CD1c^{+} DCs, and CD66^{+} granulocytes. This confirmed H3 citrullination

is induced by endogenous TLR stimulation and does not require cell-cell interaction and humoral factors derived from other immune cell subsets.

3.7. H3 citrullination and PAD4 expression is enhanced in CD14^{hi} monocytes following TLR stimulation

To further confirm H3 citrullination in CD14^{hi} monocytes, we performed western blotting of sorted CD14^{hi} monocytes from three HC, three ARI, and four RA. Sorted CD14^{hi} monocytes were incubated with PBS or R848 and analyzed by western blotting (Figure S8). Cit-H3 level was normalized against total H3 level and their fold change following R848 stimulation were calculated. We found four-fold higher H3 citrullination level in stimulated CD14^{hi} monocytes from the three study groups (Figure S8A/D/G). PAD2 and PAD4 is known to be expressed in lymphocytes and catalyze the process of protain citrullination. Normalized PAD4 and PAD2 levels following R848 simulation were determined using the same ten samples above. PAD4 expression was ~1.4 times enhanced in R848 stimulated CD14^{hi} monocytes (Figure S8B/E/H), but there was no consistant change in PAD2 expression following R848 stimulation (Figure S8C/F/I), suggesting a role of PAD4 in the H3 citrullination process.

3.8. TLR stimulation induces MET formation in CD14^{hi} monocytes

Because H3 citrullination has been linked to extracellar trap formation of monocytes, we examined morphologic changes in CD14^{hi} monocytes by immunofluorescence staining and live cell imaging. Sorted CD14^{hi} monocytes in freshly drawn blood from six additional ACPA (+) ARI were analyzed. Sorted CD14^{hi} monocytes showed condensed nuclear changes with cit-H3 and PAD4 staining following R848 stimulation at three hours (Figure 4A). After four hours, stimulated CD14^{hi} monocytes showed extrusion of DNA with high cit-H3 staining, which was consistent with MET formation in previous reports [11, 25]. PAD4 expression was diminished at this time point and this seems to be due to release of PAD4 into the supernatant. These changes were not observed in unstimulated monocytes.

To quantify MET formation by an unbiased manner, we applied the method of live cell imaging to quantify MET formation by IncuCytes ZOOM. Unstimulated CD14^{hi} monocytes were unchanged. CD14^{hi} monocytes stimulated with LPS or R848 showed nuclear decondensation at three hours, followed by disrupted nuclear membranes and eventual cell membrane permeability with subsequesnt staining with sytox green dye at four hours (Figure 4B). The number of Sytox green positive cells were counted in an automated manner. Significant elevation of Sytox green positive cells following LPS and R848 stimulation compared to PBS condition was observed (Figure 4C). This confirmed induction of MET formation following TLR engagement.

3.9. TLR stimulation enhances H3 citrullination with TNFα production

We confirmed MET formation of TLR stimulated CD14^{hi} monocytes. We compared TLR stimulation with other known NETs inducers including PMA and Ionomycin [14]. PMA induced similar frequencies of H3 citrullination compared to LPS and R848 although PMA did not induce TNFα production in these cit-H3^{hi} population (Figure S9B/C). Ionomycin induced less frequent H3 citrullination without TNFα production. This confirmed that

METosis induced by TLR pathway could contribute to local inflammatory processes through release of proinflammatry cytokiens, such as TNFα.

3.10. H3 citrullination with TNFα production in CD14^{hi} monocytes is PAD4 dependent

We next sought to evaluate the relationship between H3 citrullination and TNFα upregulation using specific inhibitors which were reported to inhibit NET formation [55]. Cryopreserved PBMCs from additional six ACPA (+) ARI who were analyzed for MET formation and from six additional HC were thawed and stimulated by R848 after pretreatment with BB-Cl-Amidine (pan-PAD inhibitor), GSK484 (PAD4 inhibitor), AMF30a (PAD2 inhibitor), 3-BP (hexokinase-2 inhibitor), or DPI (NADPH oxidase inhibitor) at indicated concentration to determine effects on H3 citrullination, TNFα production, and IL-1β production in CD14^{hi} monocytes by flow cytometry analysis. We first examined cell viability and apoptosis of CD45^{+} lymphocytes in PBMC after six hour incubation with DMSO or inhibitors. There were no significant effects on cell viability or apoptosis following incubation with R848 and inhibitors (Figure S11).

In agreement with the mass cytometry analysis, we found significant H3 citrullination in CD14^{hi} monocytes (Figure 5A/C) and these cit-H3^{hi}CD14^{hi} monocytes produced TNFα but less IL-1β compared to cit-H3^{low}CD14^{hi} monocytes following R848 stimulation (Figure 5B/D). Cit-H3^{low}CD14^{hi} monocytes produced both TNFα and IL-1β following R848 stimulation. We also analyzed cell viability and apoptosis of stimulated CD14^{hi} monocytes. Cit-H3^{hi} population showed slight increase of dead cell staining which suggest cell membrane permeability consistent with MET formation without induction of apoptosis (Figure S11).

Frequencies of each population within total CD14^{hi} monocytes were normalized against frequencies in R848 condition without inhibitors. The frequency of cit-H3^{hi}CD14^{hi} monocytes was significantly decreased by BB-Cl-Amidine and GSK484 but not by AMF30a. 3-BP and DPI had no significant effects on H3 citrullination (Figure 5C). Total TNFα production was slightly inhibited by GSK484 but not by other inhibitors (Figure 5D), and these inhibitors had no effect on IL-1β production (Figure 5E).

Most of cit-H3^{hi}CD14^{hi} monocytes produced TNFα. Frequency of cit-H3^{hi} TNFα producing cells was significantly decreased by BB-Cl-Amidine and GSK484, but not by the others (Figure 5F). None of these inhibitors had suppressive effect on frequency of cit-H3^{low}TNFα producing cells (Figure 5G). CD14^{hi} monocytes from six HC showed the same result as ARI (data not shown).

These data suggest the exsistence of at least two distinct pathways in CD14^{hi} monocytes following TLR stimulation -- one that is PAD4 dependent and characterized by histone H3 citrullination with TNFα production, and another that is PAD4 independent and is unrelated to H3 citrullination (Figure 6).

4. Discussion

In sum, following TLR stimulation CD14^{hi} monocytes and CD1c^{+} DC peripheral blood cell subsets demonstrate increased H3 citrullination levels (cit-H3^{hi}), which is associated with a cytokine/chemokine/metabolomic signature. In addition, the frequency of cit-H3^{hi}CD14^{hi} monocytes was significantly increased in ARI compared to HC. This monocytic signature was most evident following TLR stimulation, exhibiting increased cytokine production such as TNFα, MIP1β, IFNα, and partially IL-12, which is a pro-inflammatory phenotype. Additionally, this cit-H3^{hi}CD14^{hi} monocyte population morphologically forms METs *ex vivo* through a process that is mediated by PAD4.

We confirmed that H3 citrullination in CD14^{hi} monocytes, CD1c^{+} DCs, and neutrophils was induced by endogenous engagement of the TLR pathway, as stimulation of these sorted populations reproduced the increased levels of H3 citrullination and the cytokine signature. This change is not found across all immune cell subsets, as cit-H3^{hi} cells were only significantly increased in ARI in the CD14^{hi} monocyte population following TLR stimulation. As there were no differences at baseline, it is likely that circulating CD14^{hi} monocytes in ARI are poised, or pre-conditioned through the effects of *PADI4* SNPs [21], potentially TLR expression levels, epigenetic modification and/or cellular metabolomic status, to respond in an enhanced manner to stimulation. These factors are not yet evaluated in ARI but are important considerations for future studies.

Importantly, similar factors have been shown to be present in ARI and RA patients and could be a consequence of this activation process. For example, multiple pro-inflammatory cytokine/chemokine elevations associate with serum ACPA (+) status in at-risk individuals [1, 5, 6]. Likewise, elevated IFN signatures [56] and the presence of ACPA and immune complexes in the periphery are potential enhancers. ACPAs could enhance monocyte function by direct interaction against cell membrane expressed citrullinated proteins [57] or by Fc receptor stimulation with ACPA binding immune complexes [58, 59]. Among cytokines, TNFα and type1 IFNs are known to strongly induce netosis [60], and thus could have a similar effect on MET formation. Understanding of these potential enhancers and transcriptional mechanism is of interest to investigate therapeutic targets to prevent development of arthritis.

Additional reports suggest the relevance of our finding to the actual disease process. Of particular interest, as a new mechanism of RA pathogenesis, macrophage extracellular trap formation and PAD release in lymphoid tissue contributes to citrullination of autoantigen and ACPA generation [11]. Macrophages in the secondary lymphoid organs (SLOs) and synovial ectopic lymphoid-like structures (ELSs) express PAD4 in murine collagen induced arthritis (CIA) and synovial biopsies from RA patients [11]. The same study showed that PAD was released from activated murine and RA synovial tissue and fluid (SF) macrophages, and which functionally deiminated extracellular proteins/peptides *in vitro*. Furthermore, activated murine and SF macrophages displayed macrophage extracellular trap formation and release of intracellular cit-H3. Although we identified enhanced H3 citrullination in monocytes and it is unknown whether this dysregulation in ARI and RA

could be preserved through differentiation to macrophages, this current study supports contribution of enhanced H3 citrullination of ARI to the development of ACPA in the SLOs.

PADs play important role in RA pathogenesis through mediation of extracellular formation of neutrophils and citrullination of nuclear and cytoplasmic proteins which could be targets of ACPA. In addition, CIA studies in mice have demostrated that selective PAD4 inhibitor was enough to ameliorate arthritis without reducing total citrulline levels in the joint or autoantibody titers but with reduction of epitope spredding and complement C3 deposition in the joints [61]. It is important to note that we demonstrated that PAD4 controls immune cell function, i.e. cytokine/chemokine signatures of $CD14^{hi}$ monocytes. Cit-$H3^{hi}$ population was skewed to produce TNFα, MIP1β, IFNβ, and IL-12 support this molecular signature is pro-inflammatory and IFN inducing phenotype. A comprehensive study of the RA joint identified a unique upregulation of TLR8 pathway and TNFα of synovial monocytes [35]. Finally, cit-$H3^{hi}$ monocytes exhibit similar molecular signature to the IFN phenotype identified in this RA joint study.

In other cell types and stimulation conditions, PAD4 and PAD2 control immune cell function through citrullination of transcriptional factors. For example, PAD4 catalyzes citrullination of NF-κB p65 and controll TNFα and IL-1β production by neutrophils [62]. In T cells, PAD2 control Th2/Th17 balance through citrullinattion of key transcriptional factors, RORγt and GATA3 [63]. Futher study is needed to investigte molecular mechanism and PTM beyond citrullination in TLR stimulated $CD14^{hi}$ monocytes.

There are some limitations to this study. This is a cross-sectional study and only one ARI eventually developed classified RA in the limited time frame studied after sample acquisition. In this context, longitudinal studies are needed to understand the significance of our findings to RA development.

In conclusion, dysregulated cytokine production as well as MET formation in $CD14^{hi}$ monocytes in ACPA (+) ARI likely plays an important role in the development of RA via promoting and perpetuating inflammation and generation of citrullinated autoantigens.

Supplementary Material

Refer to Web version on PubMed Central for supplementary material.

ACKNOWLEDGEMENTS

We would like to thank to study participants. We also thank Karen Helm and Christine Childs from the cancer center flow core shared resources for the assistance of Helios analysis, Scott Beard from Barbara Davis center for the childhood diabetes cytometry core facility for the assistance with flow cytometry analysis, Radu Moldovan, PhD at Advanced light microscopy core facility with immunofluorescence analysis.

Funding: This work was supported by the National Institutes of Health (NIH) [grant numbers AR066712, AI101981, AI130830, K23AR070897], Pfizer ASPIRE Investigator-Initiated Research Grant, Boettcher Foundation Webb-Waring Early Investigator Award

REFERENCES:

[1]. Sokolove J et al., “Autoantibody epitope spreading in the pre-clinical phase predicts progression to rheumatoid arthritis,” (in eng), PLoS One, vol. 7, no. 5, p. e35296, 2012, doi: 10.1371/journal.pone.0035296. [PubMed: 22662108]

[2]. Nielen MM et al., “Specific autoantibodies precede the symptoms of rheumatoid arthritis: a study of serial measurements in blood donors,” (in eng), Arthritis Rheum, vol. 50, no. 2, pp. 380–6, 2 2004, doi: 10.1002/art.20018. [PubMed: 14872479]

[3]. Majka DS et al., “Duration of preclinical rheumatoid arthritis-related autoantibody positivity increases in subjects with older age at time of disease diagnosis,” (in eng), Ann Rheum Dis, vol. 67, no. 6, pp. 801–7, 6 2008, doi: 10.1136/ard.2007.076679. [PubMed: 17974596]

[4]. Gerlag DM et al., “EULAR recommendations for terminology and research in individuals at risk of rheumatoid arthritis: report from the Study Group for Risk Factors for Rheumatoid Arthritis,” (in eng), Ann Rheum Dis, vol. 71, no. 5, pp. 638–41, 5 2012, doi: 10.1136/annrheumdis-2011-200990. [PubMed: 22387728]

[5]. Deane KD et al., “The number of elevated cytokines and chemokines in preclinical seropositive rheumatoid arthritis predicts time to diagnosis in an age-dependent manner,” (in eng), Arthritis Rheum, vol. 62, no. 11, pp. 3161–72, 11 2010, doi: 10.1002/art.27638. [PubMed: 20597112]

[6]. Kokkonen H, Söderström I, Rocklöv J, Hallmans G, Lejon K, and Rantapää Dahlqvist S, “Up-regulation of cytokines and chemokines predates the onset of rheumatoid arthritis,” (in eng), Arthritis Rheum, vol. 62, no. 2, pp. 383–91, 2 2010, doi: 10.1002/art.27186. [PubMed: 20112361]

[7]. van de Sande MG et al., “Different stages of rheumatoid arthritis: features of the synovium in the preclinical phase,” (in eng), Ann Rheum Dis, vol. 70, no. 5, pp. 772–7, 5 2011, doi: 10.1136/ard.2010.139527. [PubMed: 21177292]

[8]. Bemis EA et al., “Complement and its environmental determinants in the progression of human rheumatoid arthritis,” (in eng), Mol Immunol, vol. 112, pp. 256–265, 8 2019, doi: 10.1016/j.molimm.2019.05.012. [PubMed: 31207549]

[9]. Holers VM et al., “Rheumatoid arthritis and the mucosal origins hypothesis: protection turns to destruction,” (in eng), Nat Rev Rheumatol, vol. 14, no. 9, pp. 542–557, 9 2018, doi: 10.1038/s41584-018-0070-0. [PubMed: 30111803]

[10]. Mandik-Nayak L, Wipke BT, Shih FF, Unanue ER, and Allen PM, “Despite ubiquitous autoantigen expression, arthritogenic autoantibody response initiates in the local lymph node,” (in eng), Proc Natl Acad Sci U S A, vol. 99, no. 22, pp. 14368–73, 10 2002, doi: 10.1073/pnas.182549099. [PubMed: 12391319]

[11]. El Shikh MEM et al., “Extracellular traps and PAD4 released by macrophages induce citrullination and auto-antibody production in autoimmune arthritis,” (in eng), J Autoimmun, vol. 105, p. 102297, 12 2019, doi: 10.1016/j.jaut.2019.06.008. [PubMed: 31277965]

[12]. Okamoto Y et al. “Sputum neutrophils from individuals at-risk for RA demonstrate increased citrullinated histone H3 containing neutrophil extracellular traps that correlate with sputum anti-cyclic citrullinated peptide antibody levels,” Arthritis Rheumatol. 2018; 70 (suppl 10).

[13]. Brinkmann V et al., “Neutrophil extracellular traps kill bacteria,” (in eng), Science, vol. 303, no. 5663, pp. 1532–5, 3 2004, doi: 10.1126/science.1092385. [PubMed: 15001782]

[14]. Khan MA and Palaniyar N, “Transcriptional firing helps to drive NETosis,” (in eng), Sci Rep, vol. 7, p. 41749, 2 2017, doi: 10.1038/srep41749. [PubMed: 28176807]

[15]. Skopelja-Gardner S, Jones JD, and Rigby WFC, ““NETtling” the host: Breaking of tolerance in chronic inflammation and chronic infection,” (in eng), J Autoimmun, vol. 88, pp. 1–10, 3 2018, doi: 10.1016/j.jaut.2017.10.008. [PubMed: 29100671]

[16]. Makrygiannakis D et al., “Smoking increases peptidylarginine deiminase 2 enzyme expression in human lungs and increases citrullination in BAL cells,” (in eng), Ann Rheum Dis, vol. 67, no. 10, pp. 1488–92, 10 2008, doi: 10.1136/ard.2007.075192. [PubMed: 18413445]

[17]. Chang HH, Dwivedi N, Nicholas AP, and Ho IC, “The W620 Polymorphism in PTPN22 Disrupts Its Interaction With Peptidylarginine Deiminase Type 4 and Enhances Citrullination and

NETosis," (in eng), Arthritis Rheumatol, vol. 67, no. 9, pp. 2323–34, 9 2015, doi: 10.1002/art.39215. [PubMed: 26019128]

[18]. Odqvist L et al., "Genetic variations in A20 DUB domain provide a genetic link to citrullination and neutrophil extracellular traps in systemic lupus erythematosus," (in eng), Ann Rheum Dis, vol. 78, no. 10, pp. 1363–1370, 10 2019, doi: 10.1136/annrheumdis-2019-215434. [PubMed: 31300459]

[19]. Montgomery AB et al., "Crystal structure of Porphyromonas gingivalis peptidylarginine deiminase: implications for autoimmunity in rheumatoid arthritis," (in eng), Ann Rheum Dis, vol. 75, no. 6, pp. 1255–61, 6 2016, doi: 10.1136/annrheumdis-2015-207656. [PubMed: 26209657]

[20]. Konig MF et al., "Aggregatibacter actinomycetemcomitans-induced hypercitrullination links periodontal infection to autoimmunity in rheumatoid arthritis," (in eng), Sci Transl Med, vol. 8, no. 369, p. 369ra176, 12 2016, doi: 10.1126/scitranslmed.aaj1921.

[21]. Suzuki A et al., "Functional haplotypes of PADI4, encoding citrullinating enzyme peptidylarginine deiminase 4, are associated with rheumatoid arthritis," (in eng), Nat Genet, vol. 34, no. 4, pp. 395–402, 8 2003, doi: 10.1038/ng1206. [PubMed: 12833157]

[22]. Carmona-Rivera C et al., "Synovial fibroblast-neutrophil interactions promote pathogenic adaptive immunity in rheumatoid arthritis," (in eng), Sci Immunol, vol. 2, no. 10, 4 2017, doi: 10.1126/sciimmunol.aag3358.

[23]. Corsiero E et al., "Single cell cloning and recombinant monoclonal antibodies generation from RA synovial B cells reveal frequent targeting of citrullinated histones of NETs," (in eng), Ann Rheum Dis, vol. 75, no. 10, pp. 1866–75, 10 2016, doi: 10.1136/annrheumdis-2015-208356. [PubMed: 26659717]

[24]. Lloyd KA et al., "Differential ACPA Binding to Nuclear Antigens Reveals a PAD-Independent Pathway and a Distinct Subset of Acetylation Cross-Reactive Autoantibodies in Rheumatoid Arthritis," (in eng), Front Immunol, vol. 9, p. 3033, 2018, doi: 10.3389/fimmu.2018.03033. [PubMed: 30662440]

[25]. Granger V et al., "Human blood monocytes are able to form extracellular traps," (in eng), J Leukoc Biol, vol. 102, no. 3, pp. 775–781, 9 2017, doi: 10.1189/jlb.3MA0916-411R. [PubMed: 28465447]

[26]. Boe DM, Curtis BJ, Chen MM, Ippolito JA, and Kovacs EJ, "Extracellular traps and macrophages: new roles for the versatile phagocyte," (in eng), J Leukoc Biol, vol. 97, no. 6, pp. 1023–35, 6 2015, doi: 10.1189/jlb.4RI1014-521R. [PubMed: 25877927]

[27]. Yousefi S, Simon D, and Simon HU, "Eosinophil extracellular DNA traps: molecular mechanisms and potential roles in disease," (in eng), Curr Opin Immunol, vol. 24, no. 6, pp. 736–9, 12 2012, doi: 10.1016/j.coi.2012.08.010. [PubMed: 22981682]

[28]. Lin AM et al., "Mast cells and neutrophils release IL-17 through extracellular trap formation in psoriasis," (in eng), J Immunol, vol. 187, no. 1, pp. 490–500, 7 2011, doi: 10.4049/jimmunol.1100123. [PubMed: 21606249]

[29]. Loures FV et al., "Recognition of Aspergillus fumigatus hyphae by human plasmacytoid dendritic cells is mediated by dectin-2 and results in formation of extracellular traps," (in eng), PLoS Pathog, vol. 11, no. 2, p. e1004643, 2 2015, doi: 10.1371/journal.ppat.1004643. [PubMed: 25659141]

[30]. Pierer M, Wagner U, Rossol M, and Ibrahim S, "Toll-like receptor 4 is involved in inflammatory and joint destructive pathways in collagen-induced arthritis in DBA1J mice," (in eng), PLoS One, vol. 6, no. 8, p. e23539, 2011, doi: 10.1371/journal.pone.0023539. [PubMed: 21858160]

[31]. Jung YO et al., "Synergism of toll-like receptor 2 (TLR2), TLR4, and TLR6 ligation on the production of tumor necrosis factor (TNF)-alpha in a spontaneous arthritis animal model of interleukin (IL)-1 receptor antagonist-deficient mice," (in eng), Immunol Lett, vol. 123, no. 2, pp. 138–43, 4 2009, doi: 10.1016/j.imlet.2009.03.004. [PubMed: 19428561]

[32]. Brentano F, Schorr O, Gay RE, Gay S, and Kyburz D, "RNA released from necrotic synovial fluid cells activates rheumatoid arthritis synovial fibroblasts via Toll-like receptor 3," (in eng), Arthritis Rheum, vol. 52, no. 9, pp. 2656–65, 9 2005, doi: 10.1002/art.21273. [PubMed: 16142732]

[33]. Tamaki Y et al., “Expression of Toll-like receptors and their signaling pathways in rheumatoid synovitis,” (in eng), J Rheumatol, vol. 38, no. 5, pp. 810–20, 5 2011, doi: 10.3899/jrheum.100732. [PubMed: 21324962]

[34]. Roelofs MF et al., “The expression of toll-like receptors 3 and 7 in rheumatoid arthritis synovium is increased and costimulation of toll-like receptors 3, 4, and 7/8 results in synergistic cytokine production by dendritic cells,” (in eng), Arthritis Rheum, vol. 52, no. 8, pp. 2313–22, 8 2005, doi: 10.1002/art.21278. [PubMed: 16052591]

[35]. Zhang F et al., “Defining inflammatory cell states in rheumatoid arthritis joint synovial tissues by integrating single-cell transcriptomics and mass cytometry,” (in eng), Nat Immunol, vol. 20, no. 7, pp. 928–942, 7 2019, doi: 10.1038/s41590-019-0378-1. [PubMed: 31061532]

[36]. Kolfenbach JR et al., “A prospective approach to investigating the natural history of preclinical rheumatoid arthritis (RA) using first-degree relatives of probands with RA,” (in eng), Arthritis Rheum, vol. 61, no. 12, pp. 1735–42, 12 2009, doi: 10.1002/art.24833. [PubMed: 19950324]

[37]. Hughes-Austin JM et al., “Multiple cytokines and chemokines are associated with rheumatoid arthritis-related autoimmunity in first-degree relatives without rheumatoid arthritis: Studies of the Aetiology of Rheumatoid Arthritis (SERA),” (in eng), Ann Rheum Dis, vol. 72, no. 6, pp. 901–7, 6 2013, doi: 10.1136/annrheumdis-2012-201505. [PubMed: 22915618]

[38]. Aletaha D et al., “2010 Rheumatoid arthritis classification criteria: an American College of Rheumatology/European League Against Rheumatism collaborative initiative,” (in eng), Arthritis Rheum, vol. 62, no. 9, pp. 2569–81, 9 2010, doi: 10.1002/art.27584. [PubMed: 20872595]

[39]. Begovich AB et al., “A missense single-nucleotide polymorphism in a gene encoding a protein tyrosine phosphatase (PTPN22) is associated with rheumatoid arthritis,” (in eng), Am J Hum Genet, vol. 75, no. 2, pp. 330–7, 8 2004, doi: 10.1086/422827. [PubMed: 15208781]

[40]. Orozco G et al., “Association of a functional single-nucleotide polymorphism of PTPN22, encoding lymphoid protein phosphatase, with rheumatoid arthritis and systemic lupus erythematosus,” (in eng), Arthritis Rheum, vol. 52, no. 1, pp. 219–24, 1 2005, doi: 10.1002/art.20771. [PubMed: 15641066]

[41]. O’Gorman WE et al., “Single-cell systems-level analysis of human Toll-like receptor activation defines a chemokine signature in patients with systemic lupus erythematosus,” (in eng), J Allergy Clin Immunol, vol. 136, no. 5, pp. 1326–36, 11 2015, doi: 10.1016/j.jaci.2015.04.008. [PubMed: 26037552]

[42]. O’Gorman WE et al., “Mass cytometry identifies a distinct monocyte cytokine signature shared by clinically heterogeneous pediatric SLE patients,” (in eng), J Autoimmun, 4 2017, doi: 10.1016/j.jaut.2017.03.010.

[43]. Baxter RM, Kong DS, Garcia-Perez JE, O’Gorman WE, and Hsieh EWY, “Single-cell Analysis of Immunophenotype and Cytokine Production in Peripheral Whole Blood via Mass Cytometry,” (in eng), J Vis Exp, no. 136, 6 2018, doi: 10.3791/57780.

[44]. Finck R et al., “Normalization of mass cytometry data with bead standards,” (in eng), Cytometry A, vol. 83, no. 5, pp. 483–94, 5 2013, doi: 10.1002/cyto.a.22271. [PubMed: 23512433]

[45]. Schuyler RP et al., “Minimizing Batch Effects in Mass Cytometry Data,” (in eng), Front Immunol, vol. 10, p. 2367, 2019, doi: 10.3389/fimmu.2019.02367. [PubMed: 31681275]

[46]. Levine JH et al., “Data-Driven Phenotypic Dissection of AML Reveals Progenitor-like Cells that Correlate with Prognosis,” (in eng), Cell, vol. 162, no. 1, pp. 184–97, 7 2015, doi: 10.1016/j.cell.2015.05.047. [PubMed: 26095251]

[47]. Toghi Eshghi S et al., “Quantitative Comparison of Conventional and t-SNE-guided Gating Analyses,” (in eng), Front Immunol, vol. 10, p. 1194, 2019, doi: 10.3389/fimmu.2019.01194. [PubMed: 31231371]

[48]. Bruggner RV, Bodenmiller B, Dill DL, Tibshirani RJ, and Nolan GP, “Automated identification of stratifying signatures in cellular subpopulations,” (in eng), Proc Natl Acad Sci U S A, vol. 111, no. 26, pp. E2770–7, 7 2014, doi: 10.1073/pnas.1408792111. [PubMed: 24979804]

[49]. Witten DM and Tibshirani RJ, “Extensions of sparse canonical correlation analysis with applications to genomic data,” (in eng), Stat Appl Genet Mol Biol, vol. 8, p. Article28, 2009, doi: 10.2202/1544-6115.1470.

[50]. Ziegler-Heitbrock L et al., “Nomenclature of monocytes and dendritic cells in blood,” (in eng), Blood, vol. 116, no. 16, pp. e74–80, 10 2010, doi: 10.1182/blood-2010-02258558. [PubMed: 20628149]

[51]. Marder W et al., “Placental histology and neutrophil extracellular traps in lupus and pre-eclampsia pregnancies,” (in eng), Lupus Sci Med, vol. 3, no. 1, p. e000134, 2016, doi: 10.1136/lupus-2015-000134. [PubMed: 27158525]

[52]. Gupta S, Chan DW, Zaal KJ, and Kaplan MJ, “A High-Throughput Real-Time Imaging Technique To Quantify NETosis and Distinguish Mechanisms of Cell Death in Human Neutrophils,” (in eng), J Immunol, vol. 200, no. 2, pp. 869–879, 1 2018, doi: 10.4049/jimmunol.1700905. [PubMed: 29196457]

[53]. van de Stadt LA, Witte BI, Bos WH, and van Schaardenburg D, “A prediction rule for the development of arthritis in seropositive arthralgia patients,” (in eng), Ann Rheum Dis, vol. 72, no. 12, pp. 1920–6, 12 2013, doi: 10.1136/annrheumdis-2012-202127. [PubMed: 23178208]

[54]. Chang HH et al., “A molecular signature of preclinical rheumatoid arthritis triggered by dysregulated PTPN22,” (in eng), JCI Insight, vol. 1, no. 17, p. e90045, 10 2016, doi: 10.1172/jci.insight.90045. [PubMed: 27777982]

[55]. Khandpur R et al., “NETs are a source of citrullinated autoantigens and stimulate inflammatory responses in rheumatoid arthritis,” (in eng), Sci Transl Med, vol. 5, no. 178, p. 178ra40, 3 2013, doi: 10.1126/scitranslmed.3005580.

[56]. Lübbers J et al., “The type I IFN signature as a biomarker of preclinical rheumatoid arthritis,” (in eng), Ann Rheum Dis, vol. 72, no. 5, pp. 776–80, 5 2013, doi: 10.1136/annrheumdis-2012-202753. [PubMed: 23434571]

[57]. Lu MC et al., “Anti-citrullinated protein antibodies activated ERK1/2 and JNK mitogen-activated protein kinases via binding to surface-expressed citrullinated GRP78 on mononuclear cells,” (in eng), J Clin Immunol, vol. 33, no. 3, pp. 558–66, 4 2013, doi: 10.1007/s10875-012-9841-6. [PubMed: 23188524]

[58]. Cooper DL et al., “FcγRIIIa expression on monocytes in rheumatoid arthritis: role in immune-complex stimulated TNF production and non-response to methotrexate therapy,” (in eng), PLoS One, vol. 7, no. 1, p. e28918, 2012, doi: 10.1371/journal.pone.0028918. [PubMed: 22235253]

[59]. Laurent L et al., “Fcγ receptor profile of monocytes and macrophages from rheumatoid arthritis patients and their response to immune complexes formed with autoantibodies to citrullinated proteins,” (in eng), Ann Rheum Dis, vol. 70, no. 6, pp. 1052–9, 6 2011, doi: 10.1136/ard.2010.142091. [PubMed: 21406456]

[60]. Mantovani A, Cassatella MA, Costantini C, and Jaillon S, “Neutrophils in the activation and regulation of innate and adaptive immunity,” (in eng), Nat Rev Immunol, vol. 11, no. 8, pp. 519–31, 7 2011, doi: 10.1038/nri3024. [PubMed: 21785456]

[61]. Willis VC et al., “Protein arginine deiminase 4 inhibition is sufficient for the amelioration of collagen-induced arthritis,” (in eng), Clin Exp Immunol, vol. 188, no. 2, pp. 263–274, 05 2017, doi: 10.1111/cei.12932. [PubMed: 28128853]

[62]. Sun B et al., “Citrullination of NF-κB p65 promotes its nuclear localization and TLR-induced expression of IL-1β and TNFα,” (in eng), Sci Immunol, vol. 2, no. 12, 6 2017, doi: 10.1126/sciimmunol.aal3062.

[63]. Sun B et al., “Reciprocal regulation of Th2 and Th17 cells by PAD2-mediated citrullination,” (in eng), JCI Insight, vol. 4, no. 22, 11 2019, doi: 10.1172/jci.insight.129687.

Highlights

- TLR engagement induced histone H3 citrullination in multiple immune cell types
- Pro-inflammatory monocytes with histone H3 citrullination were newly identified
- Pro-inflammatory monocytes were enhanced in ACPA (+) at-risk via TLR stimulation
- PAD4 mediates histone H3 citrullination and cytokine production in monocytes

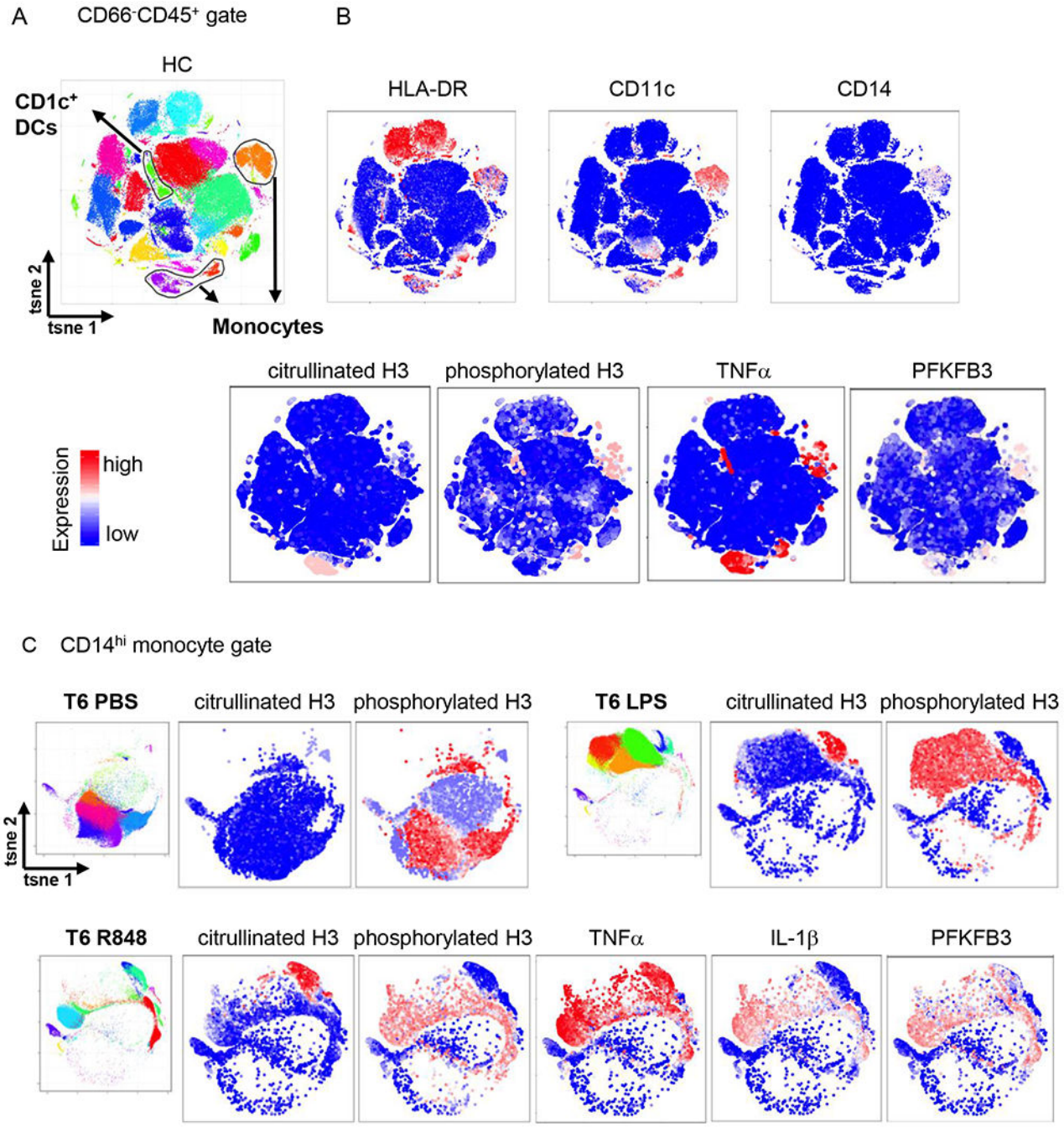

Figure 1. PhenoGraph analysis demonstrate upregulation of multiple cytokines and metabolomic molecules in CD14^{hi} monocytes and CD1c^{+} DCs with increased histone H3 modification following *ex vivo* toll-like receptor stimulation.

Whole blood samples were processed and analyzed as described in Figure S1. **Panel AB.** PhenoGraph algorism was applied to gated CD66^{-}CD45^{+} cells in the LPS and R848 conditions from HC (n=13), ACPA (+) at-risk individuals (ARI, n=13), and early RA patients (n=14). T-SNE plot was created and 42 clusters were identified. T-SNE plot of HC in the LPS condition is displayed in Panel A. Monocytes and CD1c^{+} DCs are indicated (black circles). **Panel B.** Expression of key lineage markers and intracellular molecules is

displayed. **Panel C.** Gated CD14^{hi} monocytes were analyzed by PhenoGraph and t-SNE plots were created. Twenty-six clusters were identified and t-SNE plot of each condition from ARI are displayed (multicolored). Expression of key intracellular molecules in each condition form ARI are displayed.

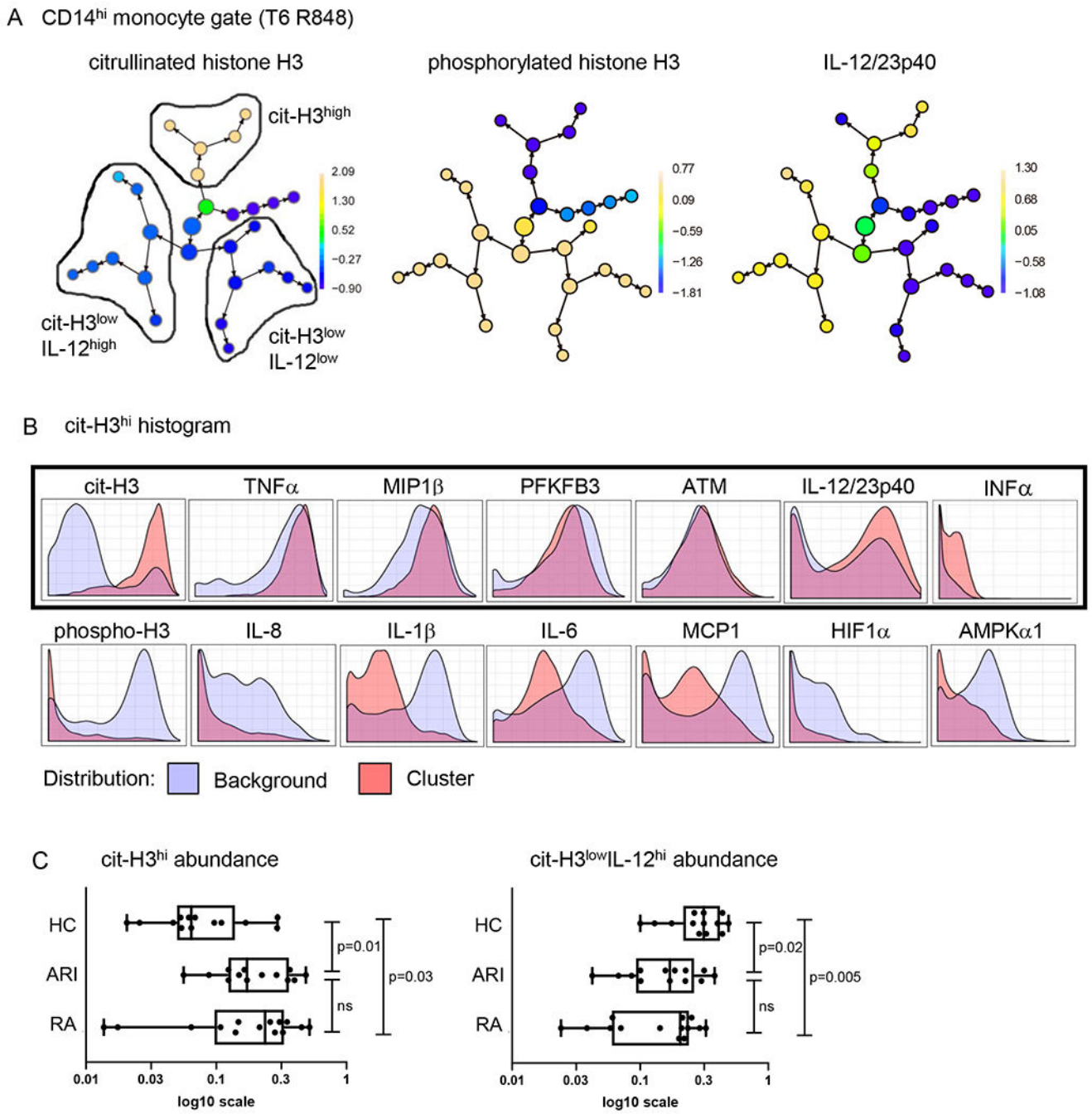

Figure 2. Subpopulations and characteristics of CD14^{hi} monocytes identified in CITRUS following *ex vivo* R848 stimulation.

Whole blood samples were processed and analyzed as described in Figure S1. Unsupervised hierarchical clustering of gated CD14^{hi} monocytes from 13 HC, 13 ACPA (+) at-risk individuals (ARI) and 14 early RA patients of R848 condition was performed. A regularized regression model (pamr) was applied to identify clusters with cytokine/metabolomics/ histone modification features. Relative expression level of each molecules in R848 condition was visualized. **Panel A.** Three distinct clusters based on relative expression level of

citrullinated histone H3 (cit-H3), phosphorylated histone H3 (phospho-H3), and IL-12/23p40 are shown in CITRUS tree. CITRUS analysis of LPS condition and other molecules for R848 condition is displayed in Figure S5/6. **Panel B.** Expression histograms of key molecules in cit-H3^{hi}CD14^{hi} monocytes are displayed. Higher expression compared to background total R848 stimulated CD14^{hi} monocytes are indicated in black square. **Panel C.** Abundance of cit-H3^{hi}CD14^{hi} monocytes and cit-H3^{low}IL-12^{hi}CD14^{hi} monocytes are depicted. Vertical lines in box indicate median level and range. P-values were calculated by Kruskal-Wallis test adjusted by Benjamini and Yekutieli method to account for multiple testing.

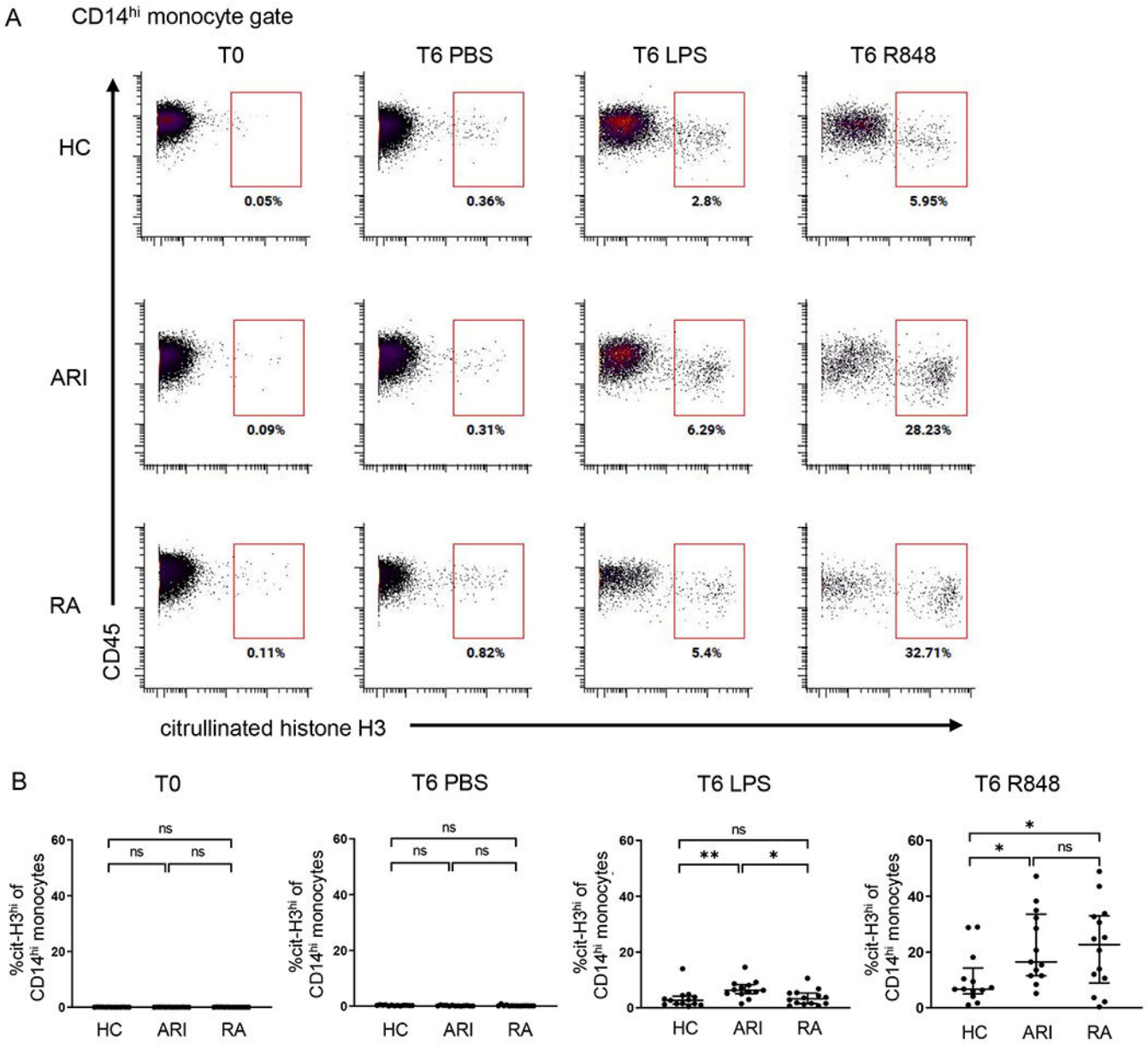

Figure 3. Enhanced histone H3 citrullination in CD14^{hi} monocytes following *ex vivo* toll-like receptor stimulation.

CD14^{hi} monocytes analyzed by mass cytometry as described in Figure S1 were gated and expression of citrullinated histone H3 (cit-H3) was manually analyzed. **Panel A.** Representative gating of cit-H3^{hi} population is shown for HC, ACPA (+) at-risk individual (ARI) and early RA patient (red square). **Panel B.** Frequencies of cit-H3^{hi}CD14^{hi} monocytes at each condition are depicted. Horizontal bars indicate median level and interquartile range. P-values were calculated by Kruskal-Wallis test adjusted by Benjamini and Yekutieli method to account for multiple testing. *p<0.05, **p<0.01.

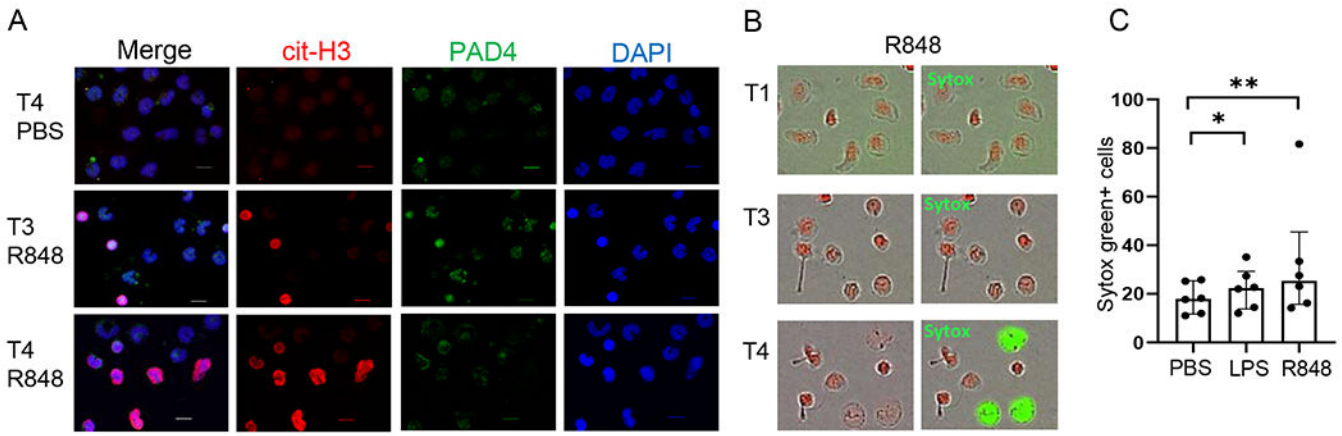

Figure 4. Extracellular trap formation in CD14^{hi} monocytes following *ex vivo* toll-like receptor stimulation.

Panel A. Sorted CD14^{hi} monocytes from ARI were cultured on coverslips with or without R848 stimulation. Cells were fixed after three hours (T3) and four hours (T4). Immunofluorescence staining was performed using DAPI, anti-cit-H3 antibody, and anti-peptidyl arginine deiminase 4 (PAD4) antibody and representative images are shown. Original magnification is 40x. Scale bars, 20 μm. **Panel B.** Sorted CD14^{hi} monocytes from ARI (n=6) were cultured on 96 well plate with or without LPS or R848 stimulation in the presence of Sytox green in the culture medium. Live cell imaging was performed by IncuCyte ZOOM and representative images at one hour (T1), three hours (T3), and four hours (T4) are shown. **Panel C.** Median number of Sytox green positive cells are depicted. Horizontal bars indicate median level and interquartile range. P-values were calculated by Friedman test adjusted by Benjamini and Yekutieli method to account for multiple testing. *p<0.05, **p<0.01.

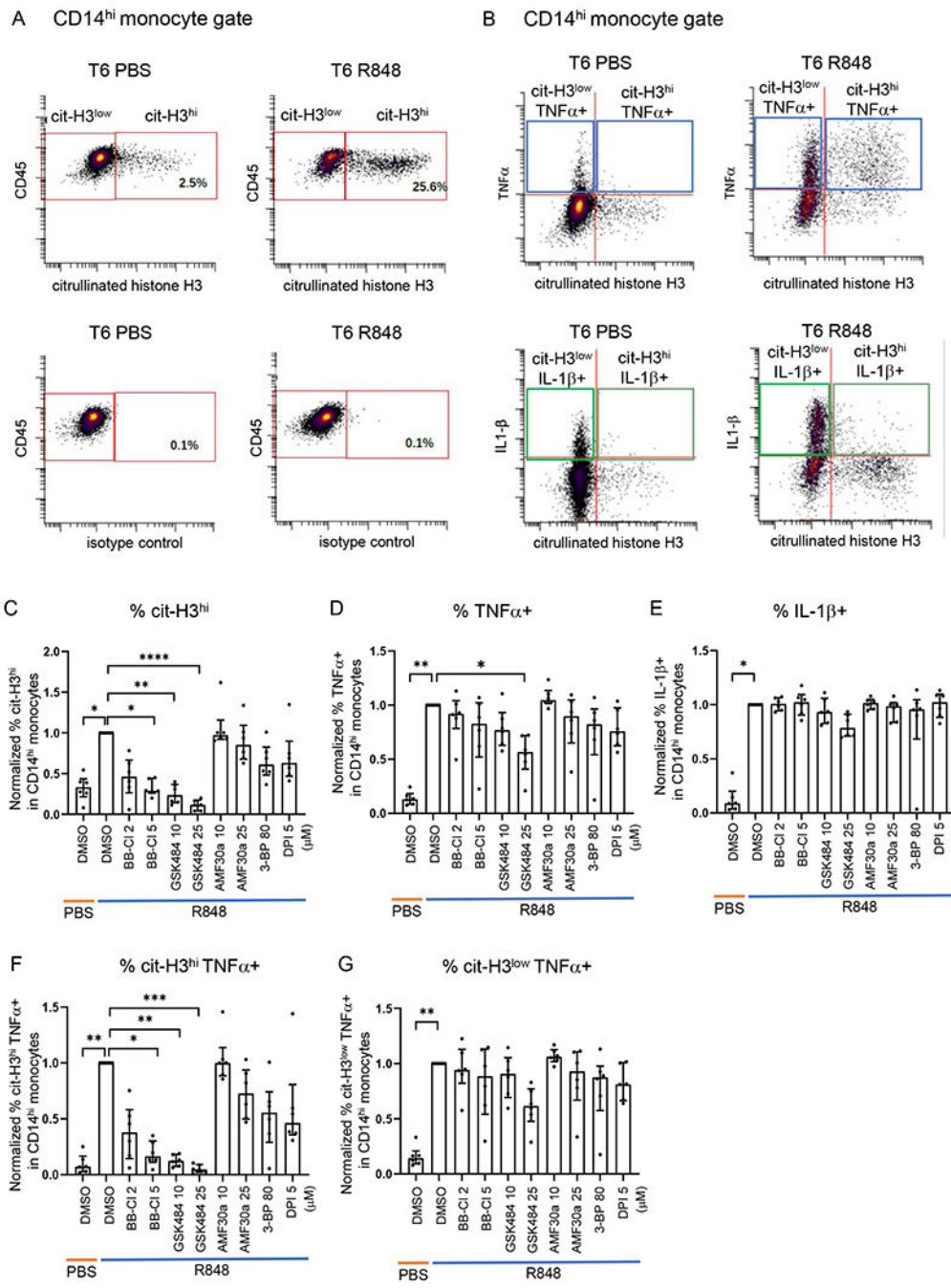

Figure 5. Endogenous responses to stimulation and suppression of histone H3 citrullination and TNFα production in CD14^{hi} monocytes by selective PAD4 inhibitor, but not by PAD2 inhibitor, without modulating IL-1β production.

CD14^{hi} monocytes from ACPA (+) at-risk individuals (n=6) were stimulated by R848 after pretreatment with BB-Cl-Amidine (pan-PAD inhibitor), GSK484 (PAD4 inhibitor), AMF30a (PAD2 inhibitor), 3-BP (bromopyruvate, hexokinase-2 inhibitor), or DPI (diphenylene iodonium, NADPH oxidase inhibitor) to determine effects on histone H3 citrullination, TNFα production, and IL-1β production by flow cytometry analysis. Cut off level was determined by 0.1% positivity of cit-H3 isotype control and 5% TNFα or IL-1β

positivity of unstimulated $CD14^{hi}$ monocytes. **Panel A.** Representative gating of citrullinated histone H3 (cit-H3)$^{hi}CD14^{hi}$ monocytes and isotype control following R848 stimulation are displayed. **Panel B.** Representative gating of TNFα producing $CD14^{hi}$ monocytes and IL-1β producing $CD14^{hi}$ monocytes are displayed. **Panel C-E.** The figures depict the normalized % of cit-$H3^{hi}CD14^{hi}$ monocytes (**Panel C**), total TNFα producing $CD14^{hi}$ monocytes (**Panel D**), and total IL-1β producing $CD14^{hi}$ monocytes (**Panel E**) by flow cytometry analysis. **Panel FG.** Normalized % of cit-$H3^{hi}$TNFα+ $CD14^{hi}$ monocytes (**Panel F**), cit-$H3^{low}$TNFα+ $CD14^{hi}$ monocytes (**Panel G**) are depicted. Horizontal bars indicate median level and interquartile range. P-values were calculated using Friedman test and adjusted by Benjamini and Yekutieli method to account for multiple testing. *$p<0.05$, **$p<0.01$, ***$p<0.001$.

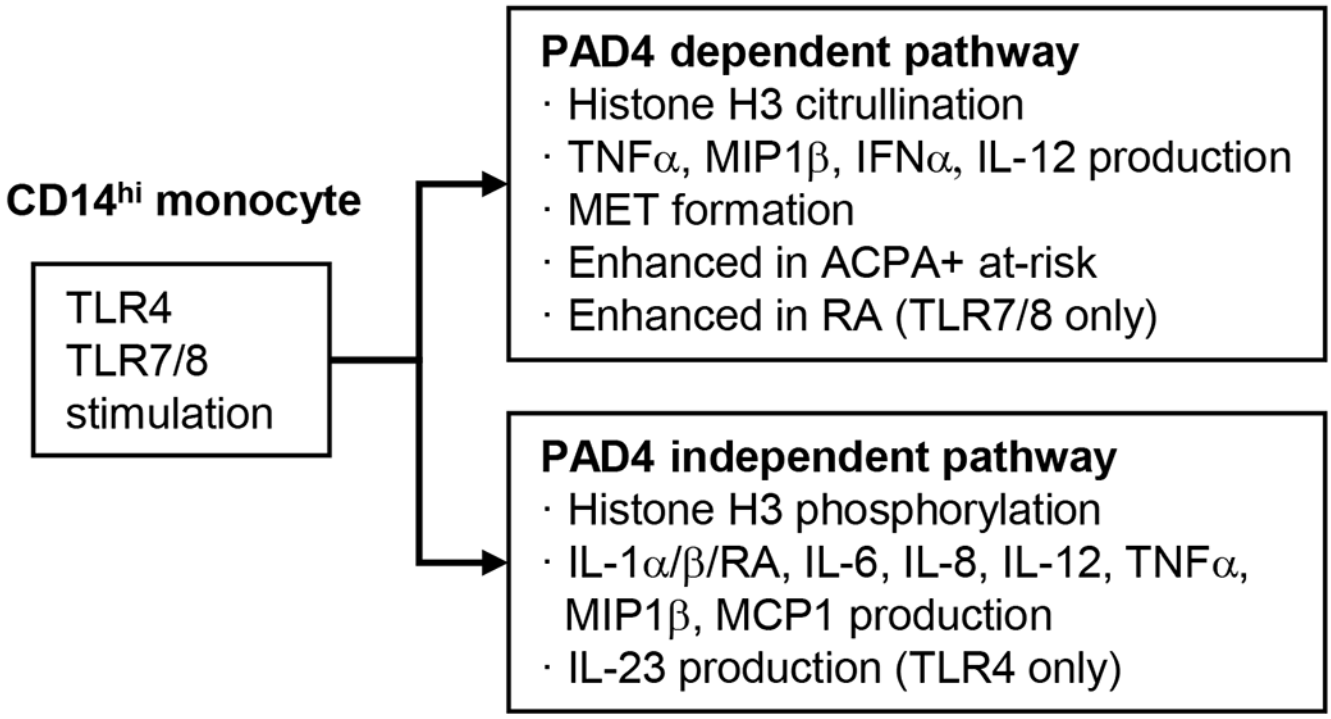

Figure 6. A proposed TLR- and PAD4- dependent pathway and its molecular signature in CD14^{hi} monocytes.

In CD14^{hi} monocytes, TLR4 and TLR7/8 stimulation induced two distinct pathways, one that is PAD4 dependent and characterized by histone H3 citrullination with TNFα production, and another that is PAD4 independent and is unrelated to H3 citrullination. Two pathways and their molecular signature are displayed.

Table 1.

Demographic characteristics of the study subjects analyzed by mass cytometry

	Controls (N=13)	At-Risk (N=13)	RA (N=14)	p-value
Age, median (range) years	54 (35-70)	62 (38-71)	50 (25-70)	0.07
Women	9 (69)	9 (69)	8 (57)	0.75
Men	4 (31)	4 (31)	6 (43)	0.75
Non-Hispanic white	12 (92)	12 (92)	8/10 (80) *	0.58
First degree relative of RA patient	0 (0)	3 (23)	3 (21)	0.19
Ever smoker	5 (38)	4 (31)	5/10 (50) *	0.65
Current smoker	0 (0)	1 (8)	3/10 (30) *	0.07
≥1 shared epitope allele	4 (31)	6 (46)	9/13 (69) **	0.09
≥1 PTPN22 single nucleotide polymorphism	5 (38)	5 (38)	2/12 (17) **	0.41
Serum CCP3.1 positivity	0 (0)	13 (100)	14 (100)	<0.00
Serum CCP3.1 titer, median (range) U/ml	5.4 (3.8-9.0)	122 (23-261.7)	261.7 (53.9-261.7)	<0.00
Serum CCP3 positivity	0 (0)	11 (85)	12 (86)	<0.00
Serum CCP3 titer, median (range) U/ml	3.8 (3.8-3.8)	84.2 (6.1-261.7)	247.2 (3.8-261.7)	<0.00
Serum RF-IgM positivity	0 (0)	4 (31)	10 (71)	<0.00
Serum RF-IgM titer, median (range) IU/ml	0.25 (0.3-3.1)	0.6 (0.25-68.7)	99.4 (0.3-105)	<0.00
Arthritis at study visit	0 (0)	0 (0)	14 (100)	<0.00
RA treatment duration, median (range), days	ND	ND	3 (0-210)	
RA treatment	None	None	Prednisone (2), Etanercept (1), Hydroxychloroquine (1), Leflunomide (1), Methotrexate (1)	

All values are number (%) unless otherwise noted.

* Four subjects lack race and smoking history

** One subject lacks SE allele and two subjects lack PTPN22 single nucleotide polymorphism data due to inadequate DNA extraction

RA; rheumatoid arthritis, PTPN22; protein tyrosine phosphatase, non-receptor type 22, CCP; Cyclic citrullinated peptide antibody, RF; rheumatoid factor

Table 2.

Three distinct clusters identified in CD14^{hi} monocytes following *ex vivo* R848 stimulation by CITRUS analysis

Cluster	Histone H3 modification	Cytokine/chemokine	Metabolomic molecule	Cluster abundance within CD14^{hi} monocytes; HC / ACPA (+) at-risk / RA
cit-H3^{hi}	Citrullination	TNFα, MIP1β, INFα, IL-12	PFKFB3	0.06 / 0.17 * / 0.24 *
cit-H3^{low}IL-12^{hi}	Phosphorylation	TNFα, MIP1β, IL-1α/1β/1RA, IL-6, IL-8, MCP1, IL-12	PFKFB3, AMPKα1	0.31 / 0.17 * / 0.21 **
cit-H3^{low}IL-12^{low}	Phosphorylation	TNFα, MIP1β, IL-1α/1β/1RA, IL-6, IL-8, MCP1	PFKFB3, AMPKα1	Not determined

Cluster abundance is compared between HC, ACPA (+) at-risk individuals and RA. P-values were calculated by Kruskal-Wallis test adjusted by Benjamini and Yekutieli method to account for multiple testing.

* $p<0.05$,

** $p<0.01$